



Cite this: *Biomater. Sci.*, 2025, **13**, 6725
Accepted 23rd September 2025

Tannin-bearing hydrogel adhesives with enhanced mechanical and adhesion strength in response to protein leakage

Joonsu Han,^a Rimsha Bhatta,^a Daniel Nguyen,^{a,b} Yusheng Liu,^a Jiadao Zhou,^a Yueji Wang,^{a,c} Dhyanes Baskaran^a and Hua Wang^{id} ^{*a,b,d,e,f,g,h}

Anastomotic leaks are among the most severe side effects following abdominal surgeries. Conventional surgical sealants and emerging hydrogel adhesives often lose mechanical and adhesion strength when exposed to leaked digestive enzymes. Here, we report a tannin-encapsulating tough hydrogel adhesive that exhibits enhanced mechanical and adhesive properties upon the encounter of leaked proteins. The hydrogel is composed of a gelatin–acrylate crosslinked network with encapsulated tannin and can adhere to a wet surface via amine–carboxyl chemistry. In the context of anastomotic leaks, tannin within the hydrogel can form a complex with proteins including the digestive enzymes, leading to increased gel stiffness and storage modulus. The enhanced mechanical strength confers improved adhesive properties on the hydrogel adhesive. Additionally, the tannin-bearing hydrogel adhesive shows excellent antibacterial properties. This adaptive and antibacterial hydrogel adhesive provides a promising sealant for gastrointestinal surgery and other applications.

Received 12th August 2025,
Accepted 23rd September 2025

DOI: 10.1039/d5bm01214g

rsc.li/biomaterials-science

Introduction

Anastomotic leaks are among the most critical complications following gastrointestinal surgeries, significantly affecting patient outcomes and life quality.^{1–3} Each year, approximately 14 million people worldwide undergo abdominal surgery to remove diseased tissues and reconnect healthy tissues using sutures or staples.⁴ Alarming, the incidence of anastomotic leaks in these patients can reach up to 19%.^{5,6} A major concern is the leakage of digestive or microbially active fluids through the reconnections, which can occur days after an initially successful surgery, leading to severe consequences

such as infection, sepsis, prolonged hospitalization, and even death.^{7–9} Notably, about 75% of anastomotic leaks are associated with colectomies,¹⁰ a procedure involving the removal of a portion of the colon. When these leakages occur in the large bowel following a colectomy, the mortality rate could be high.^{11,12} To protect the anastomosis and prevent leakage, surgeons rely on meticulous techniques such as layered closure with sutures and the use of mechanical staplers.^{13–15} However, the variability in surgical skills, potential ischemia at the suture site, and insufficient sealing all contribute to the risk of leaks.^{16–18}

As an alternative to sutures and staplers, various material-based bioadhesives have been developed to reconnect tissues and prevent leaks.^{19–23} For example, Tisseel, a fibrin sealant, has been approved by the FDA to control bleeding and prevent fluid leaks in surgeries.^{24,25} To further improve the adhesion strength, tough hydrogel adhesives with excellent mechanical strength and adhesion energy have been actively explored over the past several years.^{26,27} The tough hydrogel adhesives often form covalent bonds with the surface of tissues and possess superior abilities to dissipate the energy from the interface, thus inducing robust adhesion to wet tissues.^{28–30} However, existing surgical sealants and hydrogel adhesives often lose mechanical and adhesion strength rapidly when exposed to digestive enzymes and other metabolites in the gastrointestinal anastomotic leaks.^{31–34} Also, microbial colonization within the sealants could further deteriorate the sealing efficiency

^aDepartment of Materials Science and Engineering,
University of Illinois at Urbana-Champaign, Urbana, IL 61801, USA.
E-mail: huawang3@illinois.edu

^bDepartment of Bioengineering, University of Illinois at Urbana-Champaign, Urbana, IL 61801, USA

^cDepartment of Mechanical Science and Engineering, University of Illinois at Urbana-Champaign, Urbana, IL 61801, USA

^dCancer Center at Illinois (CCIL), Urbana, IL 61801, USA

^eCarle College of Medicine, University of Illinois at Urbana-Champaign, Urbana, IL 61801, USA

^fBeckman Institute for Advanced Science and Technology,
University of Illinois at Urbana-Champaign, Urbana, IL 61801, USA

^gMaterials Research Laboratory, University of Illinois at Urbana-Champaign, Urbana, IL 61801, USA

^hInstitute for Genomic Biology, University of Illinois at Urbana-Champaign, Urbana, IL 61801, USA



way for developing adaptive surgical sealants capable of responding to anastomotic leaks and mitigating post-surgery infections.

Results

Synthesis and characterization of TA-Gel

To synthesize TA-Gel, gelatin methacrylate, acrylic acid-*N*-hydroxysuccinimide (NHS) ester, acrylic acid, TA, and α -ketoglutaric acid were mixed and irradiated with ultraviolet (UV) light (Fig. S1a). UV radiation generated free radicals from α -ketoglutaric acid for the subsequent polymerization of acrylic acid NHS ester, gelatin methacrylate, and acrylic acid. After 20 min of UV irradiation, a clear hydrogel was formed (Fig. 2a), and the porous gel network was confirmed by scanning electron microscopy (SEM) and optical microscopic imaging (Fig. 2b and Fig. S1b). Control gels without the incorporation of TA but with all other components were also synthesized (Fig. 2c and Fig. S1b). The average porosity of TA-Gel and control gel is 9.4% and 9.5%, respectively, as per a gel

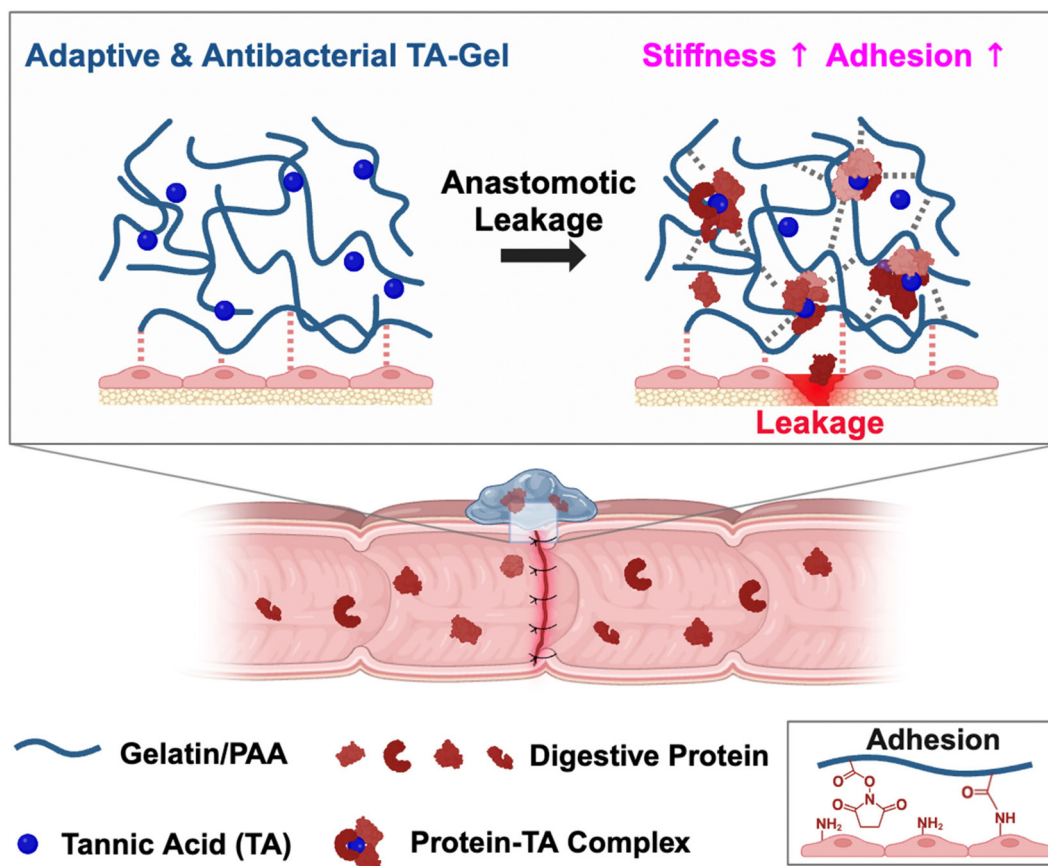


Fig. 1 Schematic illustration of TA-Gel as an adaptive and antibacterial surgical sealant responsive to anastomotic leaks. Tannic acid-containing gelatin/polyacrylic acid tough hydrogel (TA-Gel) can strongly adhere to wet tissues. Upon anastomotic leakage, TA within the hydrogel can complex with digestive enzymes in the intestinal fluid, leading to enhanced Young's modulus, stiffness, and adhesive strength (adhesive energy, tensile strength, and shear strength). TA-Gel also exhibits excellent antibacterial properties, which can be attributed to the abundant phenolic hydroxyl groups of TA, against potential bacterial infections post-leakage and during surgical procedures.

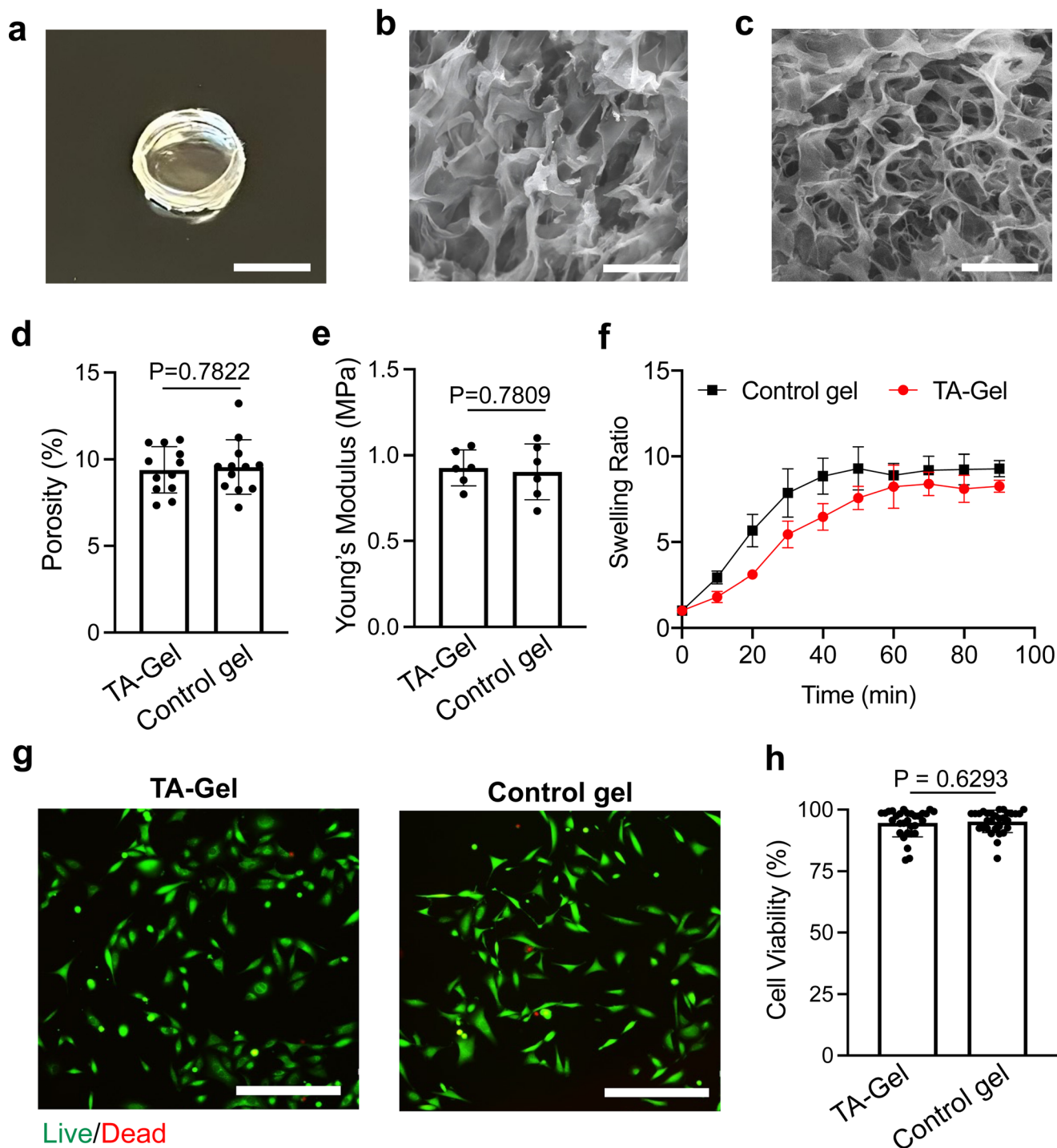


Fig. 2 Synthesis and characterization of TA-Gel. (a) Image of TA-Gel. Scale bar: 5 mm. Also shown are SEM images of (b) TA-Gel and (c) control gel. Scale bar: 4 μ m. (d) Porosity of TA-Gel and control gel. (e) Young's moduli of TA-Gel and control gel. (f) Swelling profile of dried TA-Gel or control gel in PBS at 37 $^{\circ}$ C. (g) Fluorescence images of 3T3-L1 fibroblasts cultured on TA-Gel or control gel for 48 h. Live and dead cells were stained with calcein AM and ethidium homodimer-1, respectively. Scale bar: 300 μ m. (h) Quantification of 3T3-L1 viability after being cultured on TA-Gel or control gel for 48 h. All the numerical data are presented as mean \pm SD (0.01 < $^*P \leq 0.05$; 0.001 < $^{**}P \leq 0.01$; 0.0001 < $^{***}P \leq 0.001$; $^{****}P \leq 0.0001$).

wicking assay (Fig. 2d). The Young's moduli of TA-Gel and control gel are 0.92 MPa and 0.90 MPa, respectively (Fig. 2e). We next studied the swelling properties of TA-Gel and control

gel by immersing the gels in PBS at 37 $^{\circ}$ C and monitoring the volume change of gels over time. While TA-Gel showed a slightly slower swelling process than the control gel, which



could be attributed to the denser micro-structures in the presence of TA, both gels showed a similar maximum swelling ratio (Fig. 2f). We next studied the biocompatibility of TA-Gel. 3T3-L1 fibroblasts were cultured on TA-Gel or control gel and monitored for cell survival over time (Fig. 2f). By staining live cells with Calcein AM and dead cells with Ethidium Homodimer-1 after 3 days, fibroblasts cultured on both gels showed a high viability of 94.5% and 95.1%, respectively (Fig. 2g and h). These data confirmed the negligible impact of incorporated TA on the toughness, porosity, swelling properties, and biocompatibility of gelatin hydrogels. We also ana-

lyzed the release kinetics of TA from TA-Gel, which showed <3% release of loaded TA over the course of 96 h (Fig. S2).

Adaptive properties of TA-Gel in simulated intestinal fluid (SIF)

TA with a polyphenolic structure can strongly interact with proteins *via* hydrogen bonding to form stable complexes (Fig. 3a). To assess the formation of tannin–protein complexes, we mixed TA with different concentrations (0%, 0.0125%, 0.025%, or 0.05%, w/w) of trypsin, one of the major enzymes found in the intestine. The mixture was placed in a 37 °C chamber with gentle shaking for 1 h. Compared to TA incubated with 0%

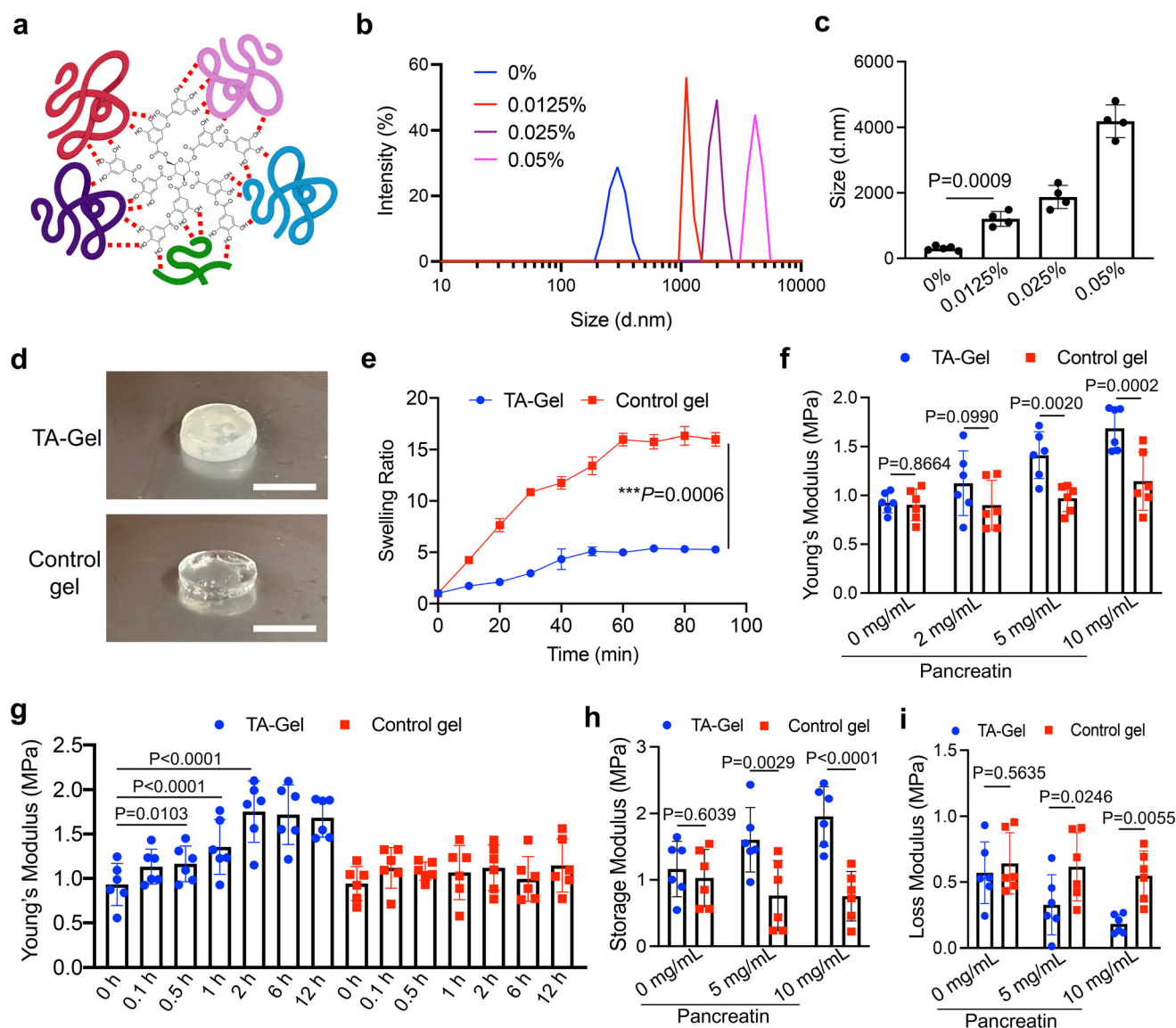


Fig. 3 Enhanced mechanical strengths of TA-Gel in response to digestive enzymes. (a) Schematic illustration of protein–TA complexes. (b) Dynamic light scattering (DLS) profiles of the mixture of TA and different concentrations (w/w) of trypsin. The mixture was placed at room temperature for 24 h prior to DLS measurements. (c) Quantified aggregate size in (b). (d) Pictures of TA-Gel and control gel after being immersed in SIF for 30 min. Scale bar: 5 mm. (e) Swelling profile of dried TA-Gel or control gel in SIF at 37 °C. (f) Young's moduli of TA-Gel and control gel after being immersed in different concentrations of pancreatin solution for 24 h. (g) Young's moduli of TA-Gel and control gel over time in SIF at 37 °C. (h) Storage moduli and (i) loss moduli of TA-Gel and control gel immersed in different concentrations of pancreatin solution for 24 h. All the numerical data are presented as mean \pm SD (0.01 < * P \leq 0.05; 0.001 < ** P \leq 0.01; 0.0001 < *** P \leq 0.001; **** P \leq 0.0001).



trypsin, the mixture of TA and trypsin formed obvious precipitates, with the number of precipitates increasing with the concentration of trypsin (Fig. S3). Dynamic light scattering (DLS) measurements also confirmed the formation of TA-trypsin complexes (Fig. 3b), and the average size of TA-trypsin complexes increased with the concentration of trypsin (Fig. 3c). We next tested the formation of TA-protein complexes within the TA-Gel, by immersing TA-Gel or control gel in the simulated intestinal fluid (SIF). Compared to the control gel that remained clear after immersion in SIF, TA-Gel rapidly became turbid (Fig. 3d), indicating the successful formation of TA-protein complexes in TA-Gel. After immersion in SIF, half-dried TA-Gel exhibited a significantly slower swelling process and a much lower maximum swelling ratio than the control gel (Fig. 3e). These data demonstrated that enzymes in SIF can diffuse into TA-Gel and form complexes with TA within TA-Gel.

To further evaluate the changes in the mechanical properties of TA-Gel due to TA-protein complex formation, TA-Gel with different TA concentrations was immersed in SIF for 24 h, and the Young's modulus was measured. The results showed that the Young's modulus of gels plateaued at a TA concentration of 10 mg mL⁻¹ (Fig. S4), which was therefore used in subsequent experiments. We next examined the effect of digestive enzymes by immersing TA-Gel or control gel in pancreatin solutions at different concentrations (0, 2, 5, and 10 mg mL⁻¹) for 24 h. In contrast to the previous finding that TA-gel or control gel immersed in PBS showed negligible differences in Young's modulus, TA-gel treated with pancreatin showed a significantly higher Young's modulus than control gel (Fig. 3f and Fig. S5). The Young's modulus of pancreatin-treated TA-Gel further increased with the concentration of pancreatin (Fig. 3f). It is noteworthy that the pristine TA-Gel and control gel already have a high Young's modulus. Therefore, the significant increase in the Young's modulus of TA-Gel after pancreatin treatment substantiated the formation of large amounts of TA-protein complexes. We also carefully monitored the change of Young's modulus of TA-Gel over time upon the treatment with pancreatin (10 mg mL⁻¹). As a result, 0.1–0.5 h incubation was sufficient to significantly increase the Young's modulus of TA-Gel (Fig. 3g). In contrast, the control gel did not show any change in the Young's modulus when immersed in a solution of pancreatin for 12 h (Fig. 3g). Compared to the control gel, TA-gel also showed a higher storage modulus (Fig. 3h) and a lower loss modulus (Fig. 3i) after the treatment with 5 or 10 mg mL⁻¹ pancreatin. These experiments demonstrated that proteins such as pancreatin can form complexes with TA in TA-Gel and lead to the increased Young's modulus and storage modulus of the gel network. The enhanced mechanical properties in the presence of TA-binding proteins make TA-Gel a promising adaptive material for responding to anastomotic leaks and other complications that involve the leakage of enzyme-containing fluids.

Enhanced bioadhesive properties of TA-Gel in response to SIF

TA-Gel, composed of a tough gelatin gel network bearing NHS groups, is also able to strongly adhere to wet tissues by

forming covalent bonds with amine-bearing tissues and dissipating energy from the adhesive interface. As TA-protein complexes can increase the Young's modulus and storage modulus of TA-Gel, we hypothesized that TA-Gel, when exposed to enzyme-containing SIF, would exhibit an enhanced energy-dissipating ability and thus an increased adhesion energy. To assess the adhesive properties of gels, the adhesion strength of TA-Gel and control gel to porcine small intestine tissues was measured using three different international standards: T peel, lap-shear, and tensile tests. TA-Gel and control gel without SIF treatment showed negligible differences in interfacial toughness (448 J m⁻² vs. 437 J m⁻²), shear strength (81 kPa vs. 83 kPa), and tensile strength (68 kPa vs. 69 kPa) (Fig. 4a–c and Fig. S6), demonstrating the minimal effect of TA on the intrinsic adhesive energy of gels. To study the impact of SIF treatment on the adhesive properties of TA-Gel, TA-Gel or control gel was adhered to porcine intestines and immersed in SIF for 24 h, followed by adhesion tests. The standard T peel test revealed an interfacial toughness of 595 J m⁻² for TA-Gel, which is significantly higher than the control gel (491 J m⁻²) and the commercial surgical sealant Tisseel (41 J m⁻²) (Fig. 4d and e). As per the lap-shear test, TA-Gel showed a shear strength of 112 kPa, which was higher than the control gel (92 kPa) and Tisseel (20 kPa) (Fig. 4f and g). Tensile tests indicated a tensile strength of 119 kPa for TA-Gel in comparison with 73 kPa for the control gel and 27 kPa for Tisseel (Fig. 4h and i). These experiments demonstrated the adaptive adhesive properties of TA-Gel, *i.e.*, enhanced adhesion energy in response to digestive enzymes in SIF.

Improved leak-proof performance of TA-Gel in response to SIF

After demonstrating that TA-Gel shows enhanced adhesion to porcine small intestine tissues in the presence of SIF, we next studied whether TA-Gel could more effectively seal intestinal leakages. To mimic the intestinal leaking conditions *in vitro*, we punched a 5 mm diameter hole in the porcine intestine and then applied TA-Gel, control gel, or Tisseel to the punched area (Fig. 5a and b). By infusing SIF or PBS into the porcine intestine that was applied with different adhesives, a burst pressure test was performed (Fig. 5a and b). When exposed to PBS, both TA-Gel and the control gel resulted in a higher burst pressure than Tisseel, and no differences between TA-Gel and control gel were observed (Fig. 5c). However, when the intestine was filled with SIF, TA-Gel resulted in a higher burst pressure than the control gel (Fig. 5d), indicating the enhanced leak-proof properties of TA-Gel in response to SIF. By extending the SIF exposure time, punched intestine tissues sealed with TA-Gel showed a stable and slightly increasing burst pressure, while the porcine tissue treated with the control gel showed a rapidly decreasing burst pressure (Fig. 5e). As a result, the difference between the TA-Gel and control gel groups became more profound with the increased SIF exposure time (Fig. 5e). These experiments further demonstrated that TA-Gel is able to adapt to the leakage of digestive fluids by improving the adhesive strength, mechanical properties, and leak-proof properties.



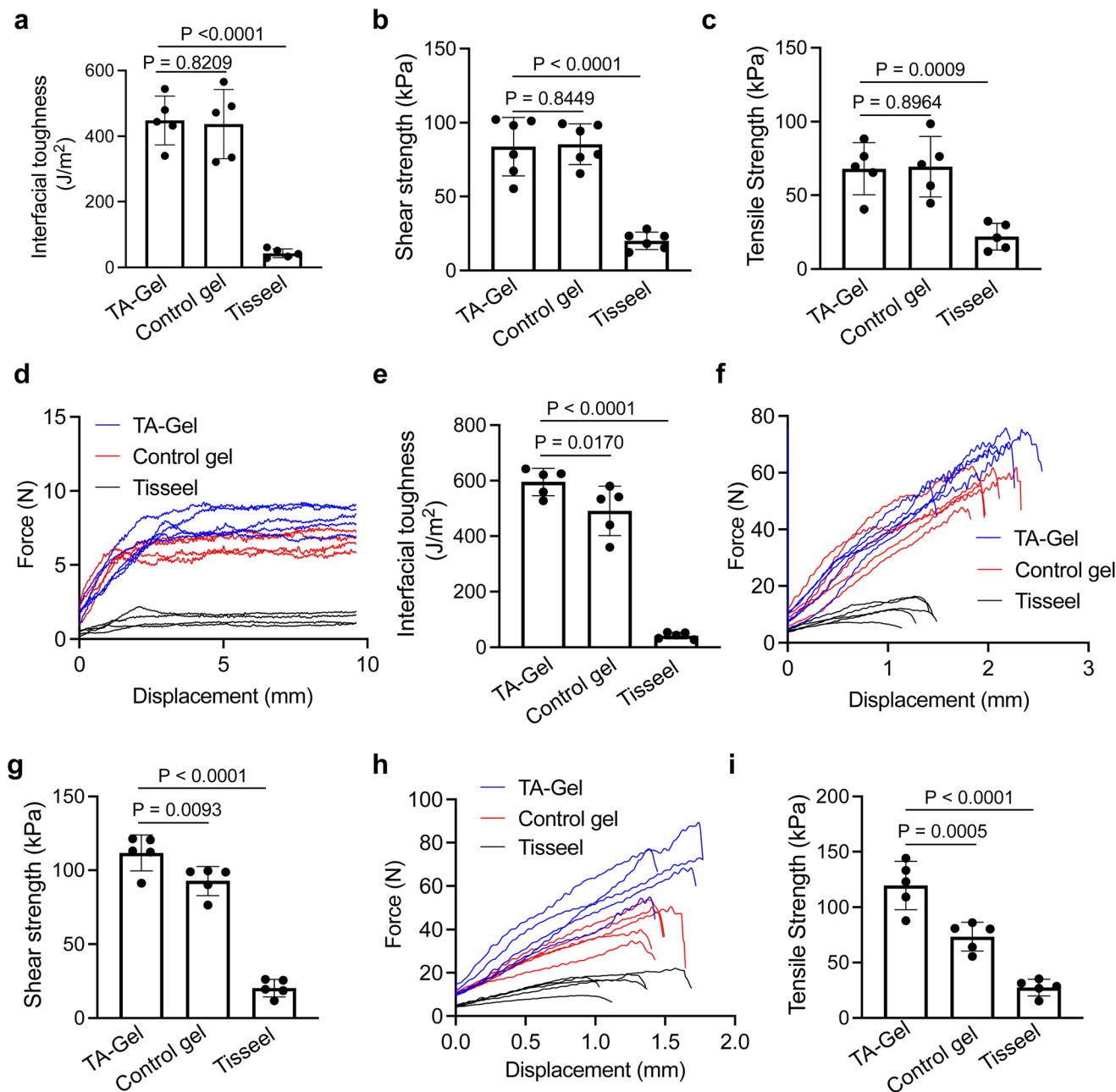


Fig. 4 Enhanced adhesive strength of TA-Gel towards wet tissues in response to intestinal fluids. (a) Interfacial toughness, (b) shear strength, and (c) tensile strength of TA-Gel, control gel, and Tisseel towards porcine intestines immersed in PBS for 24 h. (d) Force–displacement profiles and (e) interfacial toughness of TA-Gel, control gel, and Tisseel towards porcine intestines immersed in SIF for 24 h. (f) Force–displacement profiles and (g) shear strength of TA-Gel, control gel, and Tisseel towards porcine intestines immersed in SIF for 24 h. (h) Force–displacement profiles and (i) tensile strength of TA-Gel, control gel, and Tisseel towards porcine intestines immersed in SIF for 24 h. All the numerical data are presented as mean \pm SD ($0.01 < P \leq 0.05$; $0.001 < **P \leq 0.01$; $0.0001 < ***P \leq 0.001$; $****P \leq 0.0001$).

TA-Gel exhibits excellent antibacterial properties

Considering that tannin is abundant in tree bark and serves as an antibacterial barrier protecting trees from pathogens and insects, we also investigated the antibacterial properties of TA-Gel. We seeded TA-Gel, control gel, or Tisseel in 12-well plates and added the LB broth containing Gram-negative

E. coli or Gram-positive *Bacillus subtilis*. After 24 h of incubation at 37 °C, the culture media were transferred to the LB agar and incubated for an additional 24 h. A significant number of bacterial colonies were formed from the control gel group or Tisseel group (Fig. 5f and Fig. S7). In contrast, nearly no colonies were observed in the TA-Gel group, demonstrating the superior bactericidal ability of TA-Gel (Fig. 5f and Fig. S7).



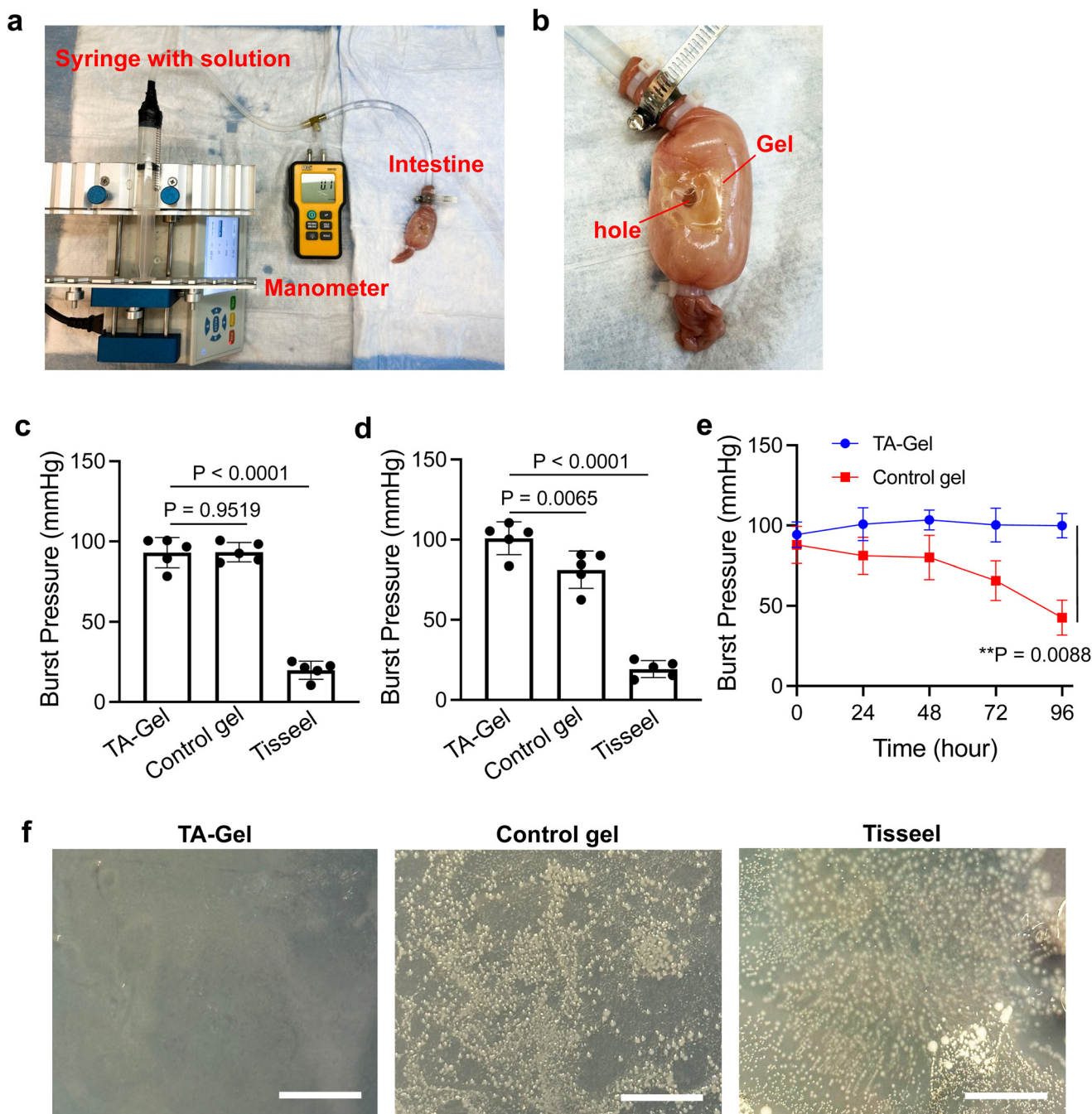


Fig. 5 TA-Gel exhibits enhanced sealing performance upon exposure to intestinal fluids and excellent antibacterial properties. (a) Experimental set-up of the burst pressure test. (b) Representative picture of TA-Gel attached to the punched hole on a porcine intestine. Shown are the measured burst pressures for porcine intestinal tissues sealed with TA-Gel, control gel, or Tisseel upon the filling of (c) PBS and (d) SIF, respectively. (e) Burst pressure of porcine intestinal tissues sealed with TA-Gel or control gel after filling with SIF for different times. (f) Representative pictures of *E. coli* colonies after being treated with TA-Gel, control gel, or Tisseel for 24 h. Scale bar: 5 mm. All the numerical data are presented as mean \pm SD ($0.01 < *P \leq 0.05$; $0.001 < **P \leq 0.01$; $0.0001 < ***P \leq 0.001$; $****P \leq 0.0001$).

The excellent antibacterial properties of TA-Gel in comparison with the control gel and conventional bioadhesives confer a high translation potential, considering the prevailing infection issues concerning surgical procedures. We also studied the immunogenicity of TA-Gel and control gel by subcutaneously implanting them into immunocompetent C57BL/6 mice and

analyzing the immune cells at the gel site after 7 days (Fig. 6a and Fig. S8). TA-Gel and control gel groups showed negligible differences in the recruitment of $CD45^+$ immune cells at the implant site (Fig. 6b). Similarly, the levels of $CD11b^+CD11c^+$ dendritic cells, $CD11b^+F4/80^+$ macrophages, and $CD11b^+Gr1^+$ neutrophils in tissues surrounding TA-Gel and control gel were



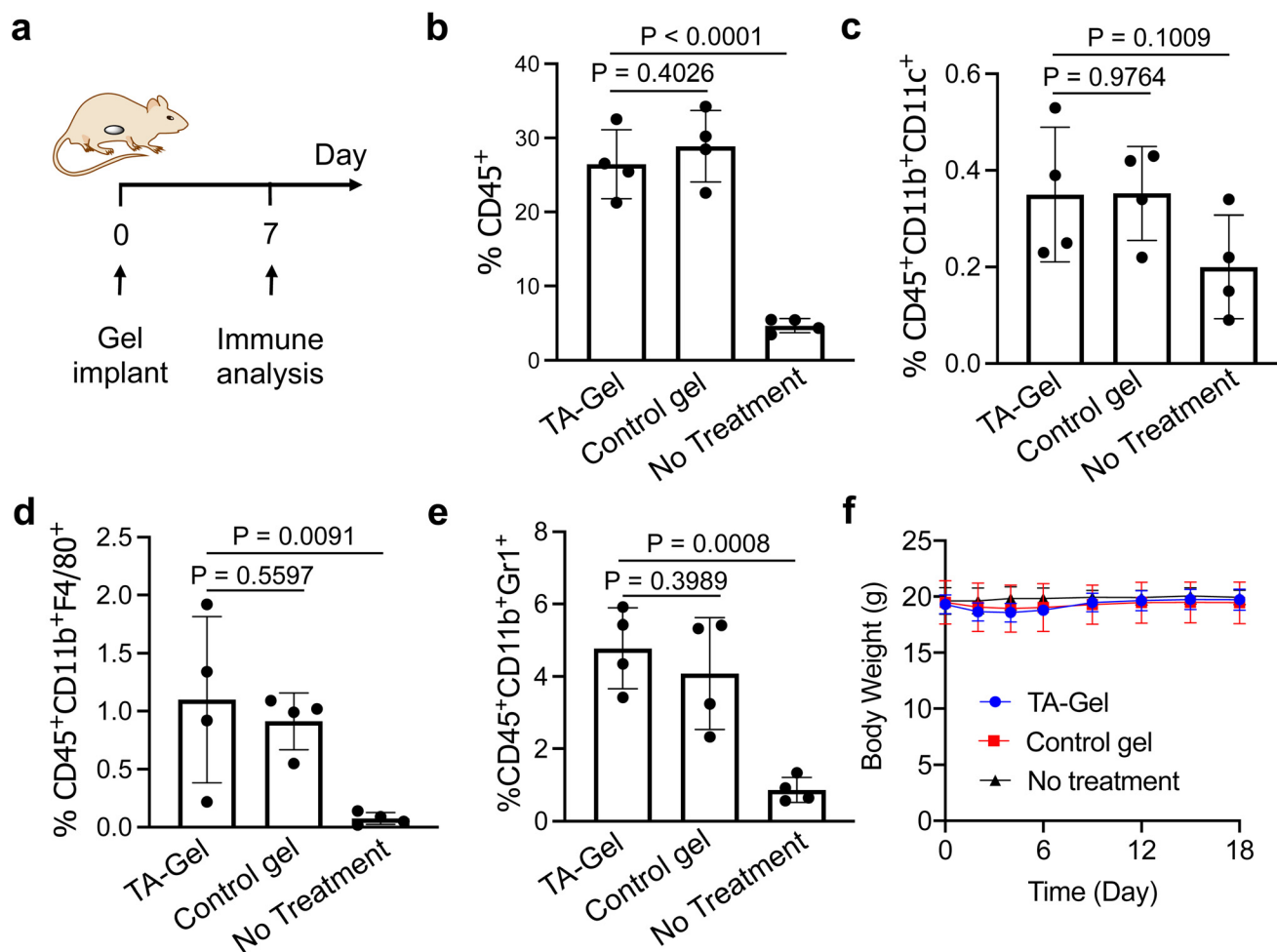


Fig. 6 TA-Gel and control gel show negligible differences in immunogenicity. (a) Timeframe of the immune analysis study. C57BL/6 mice were subcutaneously implanted with TA-Gel or control gel, followed by the analysis of immune cells in the transplant area after 7 days. (b) Percentages of CD45⁺ immune cells in skin tissues surrounding TA-Gel or control gel. (c) Percentages of CD45⁺CD11b⁺CD11c⁺ dendritic cells in skin tissues surrounding TA-Gel or control gel. (d) Percentages of CD45⁺CD11b⁺F4/80⁺ macrophages in skin tissues surrounding TA-Gel or control gel. (e) Percentages of CD45⁺CD11b⁺Gr1⁺ neutrophils in skin tissues surrounding TA-Gel or control gel. (f) Body weight of mice implanted with TA-Gel or control gel over the course of a parallel animal study. All the numerical data are presented as mean \pm SD (0.01 < **P* \leq 0.05; 0.001 < ***P* \leq 0.01; 0.0001 < ****P* \leq 0.001; *****P* \leq 0.0001).

also similar (Fig. 6c–e). The presence of immune cells at 7 days after implantation is a part of normal foreign body responses, and is expected to decay over time. Additionally, no sign of weight loss was observed for the mice implanted with TA-Gel or control gel (Fig. 6f). These experiments demonstrated that the incorporation of TA did not lead to any noticeable change in the immunogenicity of gelatin gels.

Discussion

A surgical sealant that can increase its mechanical strength and adhesion energy in response to anastomotic leakage holds great promise for gastrointestinal surgery and other applications.^{42–44} Here, we introduce a TA-bearing tough hydrogel adhesive that can improve its mechanical properties upon exposure to digestive fluids in the intestine. TA, which is

abundant in the outer layer of seeds and can form complexes with proteins due to its polyphenol structure, was incorporated during the polymerization of acrylic acid NHS ester, gelatin methacrylate, and acrylic acid to form TA-Gel. The highly cross-linked double network of gelatin and polyacrylic acid bestows a high mechanical strength on TA-Gel, with a Young's modulus of 0.9 MPa (Fig. 2e). The hydrophilic polyacrylic acids within the gel network promote the penetration of water molecules, as indicated by the high swelling ratio of TA-Gel (Fig. 2f). The presence of abundant hydrogen bonds in the gel network also contributes to the retention of TA within the gel network (Fig. S2).

TA in the TA-Gel can form complexes with digestive enzymes present in SIF (Fig. 3a–d). The formation of TA–protein complexes in the gel network confers an increased Young's modulus (Fig. 3f and g), increased storage modulus (Fig. 3h), and decreased loss modulus (Fig. 3i) on TA-Gel in



comparison with the control gel. TA-Gel and the control gel show negligible differences in the initial adhesion energy, shear strength, and tensile strength (Fig. 4a–c). However, when treated with SIF, TA-Gel exhibited a significantly higher interfacial toughness, shear strength, and tensile strength than the control gel, demonstrating the enhanced adhesive properties of TA-Gel in response to the intestinal fluid (Fig. 4d–i). As a proof-of-concept demonstration of its potential applications, we performed a burst pressure test of TA-Gel using porcine small intestines punctured with a 5 mm hole (Fig. 5a and b). While TA-Gel and the control gel showed a comparable burst pressure when filling the intestine with PBS (Fig. 5c), TA-Gel resulted in a significantly higher burst pressure compared to the control gel when filling the punctured intestine with SIF and maintained a robust burst pressure for over 4 days (Fig. 5d and e). In addition to the adaptive mechanical properties and leak-proof performance, TA-Gel also showed excellent antibacterial properties, as evidenced by its superior bactericidal effect against Gram-negative *E. coli* and Gram-positive *Bacillus subtilis* in comparison with the control gel and Tisseel (Fig. 5f and Fig. S7). These enhanced antibacterial properties could be attributed to the phenolic hydroxyl groups of TA^{45–48} and can further benefit surgery outcomes by mitigating potential post-surgical infections.

To summarize, we report an adaptive tough hydrogel adhesive (TA-Gel) that can enhance its mechanical strength and adhesion energy in response to leaked proteins. The formation of TA–protein complexes within the gel network leads to an increased Young's modulus and storage modulus for TA-Gel and thus improves the adhesion strength of TA-Gel towards leaking tissues. The burst pressure test with porcine intestines also validated the adaptive properties of TA-Gel. This adaptive tough hydrogel adhesive, with excellent antibacterial properties, provides a promising sealant for gastrointestinal surgery and other applications.

Methods

Materials

Tannic acid, gelatin, acrylic acid *N*-hydroxysuccinimide ester, acrylic acid, gelatin methacrylate, α -ketoglutaric acid, potassium phosphate monobasic, and pancreatin from porcine pancreas were purchased from Sigma-Aldrich (St Louis, MO, USA). Porcine small intestine tissues for the adhesion test and the burst pressure test were purchased from Sierra for Medical Science (Whittier, CA, USA). Poly(methyl methacrylate) films with a thickness of 50 μ m were purchased from VWR International (Radnor, PA, USA). Calcein AM and ethidium homodimer 1 were purchased from Thermo Fisher (Waltham, MA, USA). Fluorescence images were obtained using an EVOS microscope (Thermo Fisher, Waltham, MA, USA). Mechanical tests were performed with Criterion C43.104E (MTS, Eden Prairie, MN) for the adhesion test, Q800 Dynamic Mechanical Analysis (DMA) for Young's modulus, and a TA DHR-3 rheometer for rheological studies. Primary antibodies used in this

study, including Alexa Fluor 700-conjugated anti-CD45 (Invitrogen), PE-conjugated anti-CD11b (Invitrogen), fluorescein isothiocyanate (FITC)-conjugated anti-CD11c (Invitrogen), PE-conjugated anti-CD86 (Invitrogen), PerCP/Cy5.5-conjugated anti-F4/80 (Invitrogen), FITC-conjugated anti-Gr-1 (Invitrogen), and PE-Cy7-conjugated anti-MHCII (Invitrogen), were purchased from Thermo Fisher Scientific (Waltham, MA, USA). Fixable viability dye eFluor780 was obtained from Thermo Fisher Scientific (Waltham, MA, USA). All antibodies were diluted according to the manufacturer's recommendations. FACS analyses were performed on Attune NxT flow cytometers and analyzed on FCS Express v6 and v7. Statistical testing was performed using GraphPad Prism v9.

Cell line and animals

The 3T3-L1 cell line was purchased from American Type Culture Collection (Manassas, VA, USA). Cells were cultured in DMEM containing 10% FBS, 100 units per mL penicillin G and 100 μ g mL^{−1} streptomycin at 37 °C in 5% CO₂ humidified air. Female C57BL/6 mice were purchased from Jackson Laboratory (Bar Harbor, ME, USA). Feed and water were available *ad libitum*. Artificial light was provided in a 12/12 hour cycle. All procedures involving animals were carried out in compliance with the National Institutes of Health and Institutional guidelines with approval from the Institutional Animal Care and Use Committee at the University of Illinois at Urbana-Champaign.

Preparation of TA-Gel

Hydrogel formulation followed our earlier protocol.²¹ A mixture consisting of 30% (w/w) acrylic acid, 1% (w/w) tannic acid, 10% (w/w) gelatin, 1% (w/w) acrylic acid *N*-hydroxysuccinimide ester, 0.1% (w/w) gelatin methacrylate, and 0.2% (w/w) α -ketoglutaric acid was dissolved in deionized water. The mixture was poured into a PTFE mold and cured in an ultraviolet light chamber (320 nm, 60 W power) for 15 minutes. For some tests, the gels were completely dried in a 60 °C oven.

Preparation of simulated intestinal fluid

6.8 g of potassium phosphate monobasic was dissolved in 250 mL of water, followed by mixing with 190 mL of sodium hydroxide solution (0.2 M). 400 mL of water and 10 g of pancreatin were then added. After the complete dissolution, pH was adjusted to 7.5 using sodium hydroxide solution (0.2 M) and the solution was diluted with water to a total volume of 1000 mL.

SEM imaging of gels

The gels were fixed with 4% paraformaldehyde in PBS for 20 min. Following fixation, they were transferred to PBS and washed for 5 min. The gels were then dehydrated by sequential immersion in ethanol solutions of increasing concentrations (0%, 30%, 50%, 70%, 90%, and 100%) for 5 min and 10 min each. After dehydration, the gels were placed in a 1 : 1 ethanol–HMDS solution for 5 minutes, followed by two 10-minute



immersions in pure HMDS. Excess solution was removed using a Kimwipe without disrupting the gel structure. The gel structure was imaged with a Hitachi S-4800 high resolution SEM after being sputter coated with Au-Pd for 40 seconds.

Porosity measurement

TA-Gel or control gel was soaked in 1 mL of deionized water under ambient conditions. A gel wicking assay was then performed using an absorbent Kimwipe (Kimberly-Clark) that touched only one side of the gel, allowing the water within the pores to be drawn out by capillary force. The initial weight of the gel (W_i) and the final weight after the wicking assay (W_f) were measured. The porosity was then calculated as $100\% \times (W_i - W_f)/W_i$.

Young's modulus measurement

TA-Gel or control gel was prepared with the dimensions of $25 \text{ mm} \times 5 \text{ mm} \times 1 \text{ mm}$. The gels were immersed in pancreatin solution with different concentrations for 24 h. The Young's moduli were analyzed by dynamic mechanical analysis.

Storage and loss modulus measurements

TA-Gel or control gel was prepared with the dimensions of $25 \text{ mm} \times 25 \text{ mm} \times 1 \text{ mm}$. Followed by the immersion in pancreatin solution with different concentrations for 24 h, the gels were cut into a circular shape using the $\varnothing 25 \text{ mm}$ arch punch. The gels were stored in PBS prior to the analysis. The storage and loss moduli were analyzed with a DHR-3 rheometer.

Adhesion tests

Porcine small intestine tissues were sliced to the dimensions of $75 \text{ mm} \times 25 \text{ mm}$ ($l \times w$) for peeling and lap-shear tests and $25 \text{ mm} \times 25 \text{ mm}$ ($l \times w$) for the tensile test. The porcine small intestine tissues were sprayed with 0.01% (w/v) sodium azide solution to prevent degradation and dehydration and placed in a zipper bag. $50 \mu\text{m}$ poly(methyl methacrylate) films were attached to the back side of the tissues as a backing to prevent tissue deformation during the test. After washing the tissues with PBS, TA-Gel or control gel was applied onto the tissue and pressed at 1 kPa for 5 seconds. Then, the tissues adhered to the gelatin gel were immersed in simulated intestinal fluid for 24 h. To measure the interfacial toughness of gels, the tissues were tested by the standard T peel test (ASTM D1876) using an electromechanical test frame with a 200 N load cell. The peeling speed was 50 mm min^{-1} . The interfacial toughness can be calculated by dividing two times the maximum force measured by the width of the sample. To measure the shear strength, the tissues were tested by the standard lap-shear test (ASTM D5868) with the same instrumental settings. The shear strength was calculated by dividing the maximum force by the adhesion area. To measure the tensile strength, the tissues were tested by the standard tensile test (ASTM D897) with the same instrumental settings. The tensile strength was calculated by dividing the maximum force by the adhesion area.

In vitro biocompatibility test

TA-Gel or control gel was plated in 24-well plates. 3T3-L1 cells were then placed on top of the gels and incubated at 37°C for 48 h. Live and dead cells were stained with $5 \mu\text{M}$ calcein AM and ethidium homodimer-1, respectively. Fluorescence images were obtained with an EVOS microscope.

In vivo biocompatibility test

TA-Gel or control gel was freshly prepared with the dimensions of 5 mm in diameter and 0.25 mm in thickness. The gels were subcutaneously implanted into the flanks of C57BL/6 mice on day 0. The weights of the mice were closely monitored after the implantation. On day 7, the tissues surrounding the implant were harvested. Harvested tissues were treated with collagenase IV (0.5 mg mL^{-1}) for 45 min. Following the collagenase treatment, tissues were disrupted using a syringe plunger to collect single cell suspensions. The cells were then washed and stained for FACS analysis to analyze the immune cells.

Burst pressure test

The burst pressure was measured according to ASTM-F2392-04R, the Standard Test Method for Burst Strength of Surgical Sealants. The porcine small intestine was prepared with the dimensions of $75 \text{ mm} \times 25 \text{ mm}$. A 5 mm diameter hole was made by a biopsy punch. One end of the porcine small intestine was sealed using a cable tie. The gels were applied onto the hole, followed by gently pressing with a finger for 5 seconds. The intestine was then filled with PBS or simulated intestinal fluid for different times. The porcine small intestine was then connected to a syringe pump filled with PBS or simulated intestinal fluid at a speed of 20 mL min^{-1} . A digital manometer was connected along the tubes to measure the maximum pressure applied during the pumping.

Antimicrobial measurements of TA-Gel

The antimicrobial test was conducted following ISO 22196 guidelines. *E. coli* (10^3 – 10^4 cfu mL^{-1}) or *Bacillus subtilis* (10^3 – 10^4 cfu mL^{-1}) were grown aerobically for 10 hours at 37°C in sterile Luria-Bertani (LB) broth (10 g L^{-1} NaCl, 5 g L^{-1} yeast extract, and 10 g L^{-1} tryptone). After the growth period, these broths were centrifuged and resuspended in a 0.5% saline solution. The bacterial solution was then seeded into 12-well plates containing TA-Gel, control gel, or Tisseel and cultured for 24 h at 37°C without shaking. Following the 24 h incubation, a dilution series of each treatment was prepared, and $100 \mu\text{L}$ of three dilutions were plated onto sterile LB agar (LB broth + 20 g L^{-1} agar). After an additional 24 h incubation period, the number of colonies on each plate was determined.

Statistical analyses

Statistical analysis was performed using GraphPad Prism v9. Sample variance was tested using the *F* test. For samples with equal variance, the significance between the groups was analyzed by a two-tailed Student's *t* test. For samples with unequal



variance, a two-tailed Welch's *t*-test was performed. For multiple comparisons, a one-way analysis of variance (ANOVA) with *post hoc* Fisher's LSD test was used. The results were deemed significant at $0.01 < *P \leq 0.05$, highly significant at $0.001 < **P \leq 0.01$, and extremely significant at $***P \leq 0.001$.

Conflicts of interest

The authors declare no competing financial interests.

Data availability

The data supporting this article have been reported in the main figures or included as part of the supplementary information (SI). Supplementary information is available. See DOI: <https://doi.org/10.1039/d5bm01214g>.

No code or software was generated in this article.

Acknowledgements

We acknowledge the support from the National Science Foundation CAREER Award DMR 21-43673 CAR (H. W.), the National Institutes of Health R01CA274738 (H. W.), the National Institutes of Health R21CA270872 (H. W.), the Sontag Distinguished Scientist Award (H. W.), the American Cancer Society Award (H. W.), and the start-up package from the Department of Materials Science and Engineering at the University of Illinois at Urbana-Champaign and the Cancer Center at Illinois (H. W.).

References

- 1 P. T. Hernandez, R. M. Paspulati and S. Shanmugan, Diagnosis of Anastomotic Leak, *Clin. Colon Rectal Surg.*, 2021, **34**, 391–399.
- 2 F. D. McDermott, *et al.*, Systematic review of preoperative, intraoperative and postoperative risk factors for colorectal anastomotic leaks, *Br. J. Surg.*, 2015, **102**, 462–479.
- 3 A. Menni, G. Stavrou, G. Tzikos, A. D. Shrewsbury and K. Kotzampassi, Endoscopic Salvage of Gastrointestinal Anastomosis Leaks-Past, Present, and Future-A, *Narr. Review. Gastrointest. Disord.*, 2023, **5**, 383–407.
- 4 A. H. C. Anthis, *et al.*, Modular stimuli-responsive hydrogel sealants for early gastrointestinal leak detection and containment, *Nat. Commun.*, 2022, **13**, 7311.
- 5 C. T. Ellis and J. A. Maykel, Defining Anastomotic Leak and the Clinical Relevance of Leaks, *Clin. Colon Rectal Surg.*, 2021, **34**, 359–365.
- 6 E. C. Zarnescu, N. O. Zarnescu and R. Costea, Updates of Risk Factors for Anastomotic Leakage after Colorectal Surgery, *Diagnostics*, 2021, **11**, 2382.
- 7 T. McGiffin, *et al.*, Surgical management and long-term functional outcomes after anastomotic leak in patients undergoing minimally invasive restorative rectal resection and without a diverting ileostomy, *Aust. N. Z. J. Surg.*, 2022, **92**, 806–812.
- 8 J. Hammond, S. Lim, Y. Wan, X. Gao and A. Patkar, The burden of gastrointestinal anastomotic leaks: an evaluation of clinical and economic outcomes, *J. Gastrointest. Surg.*, 2014, **18**, 1176–1185.
- 9 J. H. Ryu, *et al.*, Multipurpose Intraperitoneal Adhesive Patches, *Adv. Funct. Mater.*, 2019, **29**, 1900495.
- 10 Y. W. Li, *et al.*, Very Early Colorectal Anastomotic Leakage within 5 Post-operative Days: a More Severe Subtype Needs Relaparatomy, *Sci. Rep.*, 2017, **7**, 39936.
- 11 O. Rennie, M. Sharma and N. Helwa, Colorectal anastomotic leakage: a narrative review of definitions, grading systems, and consequences of leaks, *Front. Surg.*, 2024, **11**, 1371567.
- 12 Z. A. Murrell and M. J. Stamos, Reoperation for anastomotic failure, *Clin. Colon Rectal Surg.*, 2006, **19**, 213–216.
- 13 A. Sciuto, *et al.*, Predictive factors for anastomotic leakage after laparoscopic colorectal surgery, *World J. Gastroenterol.*, 2018, **24**, 2247–2260.
- 14 M. D. Jaferi, V. Nfonam, B. Shogan and N. Hyman, Why Do Anastomoses Leak?, *J. Gastrointest. Surg.*, 2021, **25**, 2728–2731.
- 15 B. W. Liu, Y. Liu, J. R. Liu and Z. X. Feng, Comparison of hand-sewn and stapled anastomoses in surgeries of gastrointestinal tumors based on clinical practice of China, *World J. Surg. Oncol.*, 2014, **12**, 292.
- 16 N. Annabi, *et al.*, Surgical Materials: Current Challenges and Nano-enabled Solutions, *Nano Today*, 2014, **9**, 574–589.
- 17 L. K. Borden, A. Gargava and S. R. Raghavan, Reversible electroadhesion of hydrogels to animal tissues for suture-less repair of cuts or tears, *Nat. Commun.*, 2021, **12**, 1–10.
- 18 Y. Hong, *et al.*, A strongly adhesive hemostatic hydrogel for the repair of arterial and heart bleeds, *Nat. Commun.*, 2019, **10**, 1–11.
- 19 J. Li, *et al.*, Tough adhesives for diverse wet surfaces, *Science*, 2017, **357**, 378–381.
- 20 H. Yuk, *et al.*, Dry double-sided tape for adhesion of wet tissues and devices, *Nature*, 2019, **575**, 169–174.
- 21 J. Han, *et al.*, A double crosslinking adhesion mechanism for developing tough hydrogel adhesives, *Acta Biomater.*, 2022, **150**, 199–210.
- 22 A. M. Behrens, *et al.*, Biodegradable-Polymer-Blend-Based Surgical Sealant with Body-Temperature-Mediated Adhesion, *Adv. Mater.*, 2015, **27**, 8056–8061.
- 23 D. J. Smith, *et al.*, A multiphase transitioning peptide hydrogel for suturing ultrasmall vessels, *Nat. Nanotechnol.*, 2016, **11**, 95–102.
- 24 W. D. Spotnitz, Fibrin Sealant: The Only Approved Hemostat, Sealant, and Adhesive—a Laboratory and Clinical Perspective, *ISRN Surg.*, 2014, **2014**, 203943.
- 25 X. G. Zheng, F. Wang, Y. C. Su, C. Y. Xu and M. Z. Wang, Efficacy and safety of fibrin sealant application in patients



- undergoing thyroidectomy: a systematic review and meta-analysis, *BMC Surg.*, 2024, **24**, 122.
- 26 D. Gan, *et al.*, Plant-inspired adhesive and tough hydrogel based on Ag-Lignin nanoparticles-triggered dynamic redox catechol chemistry, *Nat. Commun.*, 2019, **10**, 1487.
 - 27 K. C. Wu, *et al.*, A tough bioadhesive hydrogel supports sutureless sealing of the dural membrane in porcine and ex vivo human tissue, *Sci. Transl. Med.*, 2024, **16**, eadj0616.
 - 28 X. Chen, H. Yuk, J. Wu, C. S. Nabzdyk and X. Zhao, Instant tough bioadhesive with triggerable benign detachment, *Proc. Natl. Acad. Sci. U. S. A.*, 2020, **117**, 15497–15503.
 - 29 J. Han, R. Bhatta and H. Wang, Bio-adhesive Macroporous Hydrogels for In Situ Recruitment and Modulation of Dendritic Cells, *Cell. Mol. Bioeng.*, 2023, **16**, 355–367.
 - 30 K. C. Wu, *et al.*, A tough bioadhesive hydrogel supports sutureless sealing of the dural membrane in porcine and ex vivo human tissue, *Sci. Transl. Med.*, 2024, **16**, eadj0616.
 - 31 X. Hu and M. W. Grinstaff, Advances in Hydrogel Adhesives for Gastrointestinal Wound Closure and Repair, *Gels*, 2023, **9**, 282.
 - 32 X. M. Chen, *et al.*, Hydrogel Bioadhesives with Extreme Acid-Tolerance for Gastric Perforation Repairing, *Adv. Funct. Mater.*, 2022, **32**, 2202285.
 - 33 G. M. Taboada, D. Dahis, P. Dosta, E. Edelman and N. Artzi, Sprayable Hydrogel Sealant for Gastrointestinal Wound Shielding, *Adv. Mater.*, 2024, **36**, 2311798.
 - 34 K. A. Vakalopoulos, *et al.*, Tissue adhesives in gastrointestinal anastomosis: a systematic review, *J. Surg. Res.*, 2013, **180**, 290–300.
 - 35 S. Reischl, D. Wilhelm, H. Friess and P. A. Neumann, Innovative approaches for induction of gastrointestinal anastomotic healing: an update on experimental and clinical aspects, *Langenbecks Arch. Chir.*, 2021, **406**, 971–980.
 - 36 K. Stergios, *et al.*, The potential effect of biological sealants on colorectal anastomosis healing in experimental research involving severe diabetes, *Ann. R. Coll. Surg. Engl.*, 2017, **99**, 189–192.
 - 37 B. Adamczyk, J. Simon, V. Kitunen, S. Adamczyk and A. Smolander, Tannins and Their Complex Interaction with Different Organic Nitrogen Compounds and Enzymes: Old Paradigms versus Recent Advances, *ChemistryOpen*, 2017, **6**, 610–614.
 - 38 L. Demonsais, A. Utz-Pugin, S. Loubery and L. Lopez-Molina, Identification of tannic cell walls at the outer surface of the endosperm upon Arabidopsis seed coat rupture, *Plant J.*, 2020, **104**, 567–580.
 - 39 J. P. Vanburen and W. B. Robinson, Formation of Complexes between Protein and Tannic Acid, *J. Agric. Food Chem.*, 1969, **17**, 772.
 - 40 X. Ni, Z. Yang and J. Y. Li, Scaling Behavior of Fracture Properties of Tough Adhesive Hydrogels, *ACS Macro Lett.*, 2021, **10**, 180–185.
 - 41 Y. Fujii, *et al.*, Complete abdominal wound and anastomotic leak with diffuse peritonitis closure achieved by an abdominal vacuum sealing drainage in a critical ill patient: a case report, *BMC Surg.*, 2018, **18**, 41.
 - 42 B. Suter, *et al.*, Surgical Sealant with Integrated Shape-Morphing Dual Modality Ultrasound and Computed Tomography Sensors for Gastric Leak Detection, *Adv. Sci.*, 2023, **10**, 202301207.
 - 43 L. Xu, *et al.*, Systematic Experimental Investigation on *In situ* Self-Adaptive Sealing Property of Composite Pressure-Activated Sealant for Curing Minor Tubular Leaks, *Energies*, 2020, **13**, 5597.
 - 44 M. S. Xie, *et al.*, Nano-enabled DNA supramolecular sealant for soft tissue surgical applications, *Nano Today*, 2023, **50**, 101825.
 - 45 A. Mori, C. Nishino, N. Enoki and S. Tawata, Antibacterial Activity and Mode of Action of Plant Flavonoids against *Proteus-Vulgaris* and *Staphylococcus-Aureus*, *Phytochemistry*, 1987, **26**, 2231–2234.
 - 46 T. Taguri, T. Tanaka and I. Kouno, Antimicrobial activity of 10 different plant polyphenols against bacteria causing food-borne disease, *Biol. Pharm. Bull.*, 2004, **27**, 1965–1969.
 - 47 R. Liu, *et al.*, Synthesis of New Biobased Antibacterial Methacrylates Derived from Tannic Acid and Their Application in UV-Cured Coatings, *Ind. Eng. Chem. Res.*, 2014, **53**, 10835–10840.
 - 48 J. G. M. Ucella, *et al.*, Tannin-rich bark extract of plants as a source of antimicrobial bioactive compounds: A bibliometric analysis, *S. Afr. J. Bot.*, 2022, **150**, 1038–1050.

